Monthly Notices
of the
ROYAL ASTRONOMICAL SOCIETY

MNRAS **476,** 470–481 (2018)
Advance Access publication 2018 January 29

doi:10.1093/mnras/sty222

Asteroseismology of KIC 7107778: a binary comprising almost identical subgiants

Yaguang Li,[1,2]★ Timothy R. Bedding,[2,3]★ Tanda Li,[2,3] Shaolan Bi,[1] Simon J. Murphy,[2,3] Enrico Corsaro,[4] Li Chen[1] and Zhijia Tian[5]

[1]*Department of Astronomy, Beijing Normal University, Beijng 100875, China*
[2]*Sydney Institute for Astronomy (SIfA), School of Physics, University of Sydney, NSW 2006, Australia*
[3]*Stellar Astrophysics Centre, Department of Physics and Astronomy, Aarhus University, Ny Munkegade 120, DK-8000 Aarhus C, Denmark*
[4]*INAF – Osservatorio Astrofisico di Catania, Via S. Sofia 78, I-95123 Catania, Italy*
[5]*Department of Astronomy, Peking University, Beijing 100871, China*

Accepted 2018 January 23. Received 2018 January 23; in original form 2017 July 17

ABSTRACT

We analyse an asteroseismic binary system: KIC 7107778, a non-eclipsing, unresolved target, with solar-like oscillations in both components. We used *Kepler* short cadence time series spanning nearly 2 yr to obtain the power spectrum. Oscillation mode parameters were determined using Bayesian inference and a nested sampling Monte Carlo algorithm with the DIAMONDS package. The power profiles of the two components fully overlap, indicating their close similarity. We modelled the two stars with MESA and calculated oscillation frequencies with GYRE. Stellar fundamental parameters (mass, radius, and age) were estimated by grid modelling with atmospheric parameters and the oscillation frequencies of $l = 0$, 2 modes as constraints. Most $l = 1$ mixed modes were identified with models searched using a bisection method. Stellar parameters for the two sub-giant stars are $M_{\rm A} = 1.42 \pm 0.06$ M$_\odot$, $M_{\rm B} = 1.39 \pm 0.03$ M$_\odot$, $R_{\rm A} = 2.93 \pm 0.05$ R$_\odot$, $R_{\rm B} = 2.76 \pm 0.04$ R$_\odot$, $t_{\rm A} = 3.32 \pm 0.54$ Gyr and $t_{\rm B} = 3.51 \pm 0.33$ Gyr. The mass difference of the system is ∼1 per cent. The results confirm their simultaneous birth and evolution, as is expected from binary formation. KIC 7107778 comprises almost identical twins, and is the first asteroseismic sub-giant binary to be detected.

Key words: binaries: general – stars: evolution – stars: oscillations.

1 INTRODUCTION

Binary star systems provide an ideal astronomical laboratory to study stellar structure and evolution. The fact that two components share same metal abundance and age provides powerful constraints on models. Eclipsing binaries are especially useful, since mass and radius can be directly measured from orbits and eclipses through spectroscopic observations and precise light-curve analysis (Andersen 1991).

Asteroseismology ushers in a new way to study binaries (Huber 2015), even for unresolved ones (Miglio et al. 2014), by analysing the two components separately. Determining stellar mass and radius is feasible for single stars with solar-like oscillations (e.g. Kallinger et al. 2010; Chaplin et al. 2014). Sub-giant and red-giant oscillating stars displaying p (pressure dominated in the envelope) and g (gravity dominated in the core) mixed modes (Chaplin & Miglio 2013) are good indicators of evolutionary stages. Their great sensitivity to mass and age can produce precise estimates of stellar parameters (e.g. Metcalfe et al. 2010; Benomar et al. 2012). Binary systems with pulsators can be analysed from modulation of the pulsation frequencies (Shibahashi & Kurtz 2012; Murphy et al. 2014; Murphy & Shibahashi 2015), so that system parameters can be determined with radial velocity curves simply derived through photometry.

White et al. (2017) pointed out that, until now, only five binary star systems have been detected with solar-like oscillations from both components. They are α Cen A and B (Bedding et al. 1998; Kjeldsen et al. 1999; Bouchy & Carrier 2001; Carrier & Bourban 2003), 16 Cyg A and B (KIC 12069424 and KIC 12069449; Metcalfe et al. 2012; Metcalfe, Creevey & Davies 2015), KIC 9139163 and KIC 9139151 (Appourchaux et al. 2012; Appourchaux et al. 2014), HD 177412 (KIC 7510397; Appourchaux et al. 2015), and HD 176465 (KIC 10124866, also known as Luke & Leia; White et al. 2017). The latter two systems are not resolved by *Kepler*, such that their light variations are mixed in a single time series. Both systems were analysed with one power spectrum, from which two sets of oscillation profiles were measured. Specifically, HD 177412 contains two main-sequence stars with mass difference ∼7.5 per cent,

★ E-mail: hnwilliam@hotmail.com (YL); tim.bedding@sydney.edu.au (TRB)

with separable oscillation frequency ranges, and HD 176465 contains two extremely similar main-sequence stars with mass difference ~ 3 per cent, leading to two significantly overlapping oscillation ranges. In addition, KIC 10080943 is another unresolved binary system, comprising two δ Sct/γ Dor hybrid pulsators on the main sequence (Keen et al. 2015; Schmid et al. 2015).

In this context, these binaries are not strictly 'twins' in that the masses are not equal to within 2 per cent (Lucy 2006; Simon & Obbie 2009). Twins are almost always found at small separations ($P \lesssim 25$ d, Lucy & Ricco 1979), though not all close binaries are twins. Further, they are more common among lower mass systems, both in observational data (e.g. Tokovinin 2000; Simon & Obbie 2009) and in binary star formation simulations (e.g. Bate 2009). Their importance lies in their ability to discriminate between dominant physical processes operating in pre-main-sequence binaries, as those authors have discussed.

Here we report on the widely separated twin binary system KIC 7107778, with mass difference $\sim$1 per cent based on our findings, an analogue to Luke & Leia (White et al. 2017). The system was not resolved by *Kepler* but was detected with oscillations from two stars in the mixed time series. It proves to be the first asteroseismic sub-giant binary system to be detected, with completely overlapping power spectra of two component stars. The paper will be structured as follows. Section 2 provides observations from previous literature and describes the processing of *Kepler* data. Section 3 illustrates the oscillation mode parameters. Section 4 details our asteroseismic analysis with stellar models of two stars, and is followed by discussions and conclusions in Section 5.

2 OBSERVATION AND DATA PROCESSING

KIC 7107778 is a binary system observed as a single target, with *Kepler* magnitude $K_p = 11.38$. The first realization of its binary identity was from speckle interferometry (Horch et al. 2012). The angular separation of the two stars is $\rho = 0.0288$ arcsec, measured with filters whose central wavelengths are 692 and 880 nm. The physical separation can be determined by combining luminosities from models with the apparent magnitude; however, such estimation is only approximate because the apparent magnitude is a blended contribution from both stars. We took advantage of the parallax determined from *Gaia* (Gaia Collaboration 2016), 1.74 ± 0.43 mas, to infer the distance to Earth and physical projected separation between the two stars, which are $d = 574^{+189}_{-113}$ pc, and $s = 16.52^{+5.44}_{-3.25}$ au. Note that this estimation is very approximate because *Gaia* parallaxes are not yet fully reliable at the present mission stage (see Fabricius et al. 2016). Assuming the orbit is circular, and adopting Kepler's third law, it suggests the orbital period of this system is about 39 yr. Therefore, we would not expect to analyse its orbit using radial velocity curves. On the other hand, such a wide separation means fully independent evolution without tidal effects or mass transfer. In the following analysis, we treat them as two single stars that have not interacted.

Several works have measured atmospheric parameters of this system. Effective temperatures measured by SDSS and IRFM are $T_{\rm eff} = 5129 \pm 82$ K and $T_{\rm eff} = 5045 \pm 105$ K, respectively. The binary system was also covered by the LAMOST-*Kepler* project, which used LAMOST low-resolution ($R \simeq 1800$ Å) optical spectra in the waveband of 3800–9000 Å and observed *Kepler*-field targets in 2014 September. The LAMOST Stellar Parameter Pipeline (Xiang et al. 2015) gives $T_{\rm eff} = 5149 \pm 150$ K, and metallicity [Fe/H] $= 0.11 \pm 0.10$ dex. Buchhave & Latham (2015) used the Tillinghast Reflector Echelle Spectrograph to obtain medium resolution ($R \simeq 44\,000$Å) spectra in the waveband of 3800–9100 Å at Fred Lawrence Whipple Observatory. They measured the metallicity [Fe/H] $= 0.05 \pm 0.08$ dex. However, all these observations treated two stars as one single target. We do not know to what extent the mixed value deviates from the real ones. Table 1 summarizes the observations in the literature.

Table 1. Atmospheric parameters of KIC 7107778.

Parameter	Value	Reference
$T_{\rm eff}$ (K)	5129 ± 82	Drimmel, Cabrera-Lavers & López-Corredoira (2003)
	5045 ± 105	Casagrande et al. (2010)
	5149 ± 150	Xiang et al. (2015)
[Fe/H] (dex)	0.11 ± 0.10	Xiang et al. (2015)
	0.05 ± 0.08	Buchhave & Latham (2015)

The *Kepler* mission observed the target in long-cadence mode (LC; 29.43 min sampling) over the whole mission and in short-cadence mode (SC; 58.84 s sampling) during Q2.1, Q5 and Q7–Q12 (Q represents three-month-long quarters). The pulsation frequency range is centred at 550 μHz, which is well above the Nyquist frequency of long cadence data ($\sim$283 μHz). Therefore, we only considered the short-cadence time series. We concatenated the data and processed it following García et al. (2011), correcting outliers, jumps, and drifts. Then it passed through a high-pass filter which was based on a Gaussian smooth function with a width of 1 d. This largely minimized instrumental side effects and only affected frequencies lower than $\sim$12 μHz, far below the frequency range we intended to analyse. We obtained the power spectrum by applying a Lomb–Scargle Periodogram (Lomb 1976; Scargle 1982) to the time series with a frequency resolution $\sim$0.012 μHz. The power spectrum is shown in Figs 1 and 2 in both logarithmic and linear scales.

The signature of solar-like oscillation is a Gaussian-like envelope located at $\nu_{\rm max}$, the so-called frequency of maximum power, and is comprised of numerous oscillation modes. In main-sequence stars, p-mode oscillations are approximately equally spaced in frequency, as described by the asymptotic equation with radial orders n and spherical degrees l (Tassoul 1980):

$$\nu_{nl} = \Delta\nu \left(n + \frac{l}{2} + \epsilon \right) - \delta\nu_{0l}, \tag{1}$$

where $\Delta\nu$ is the large separation, which measures the spacing of adjacent modes with the same l, $\delta\nu_{0l}$ is the small separation, and ϵ is an offset. In more evolved stars, the core will have g-mode oscillations, which are approximately equally spaced in period. The analogous asymptotic equation is specified by order n_g:

$$\Pi_{nl} = \nu_{nl}^{-1} = \Delta\Pi_l (n_g + \epsilon_g), \tag{2}$$

where $\Delta\Pi_l$ is the period spacing, and ϵ_g is an offset.

As the star evolves off the main sequence, central hydrogen depletes, and p and g mixed modes of $l \geq 1$ appear to have 'avoided crossings' (Aizenman, Smeyers & Weigert 1977), whereby oscillation frequencies are no longer equally spaced in either frequency or period. The $l = 0$ p modes are unaffected, which assisted us in determining the mean large separation $\langle\Delta\nu\rangle$ in an échelle diagram. The best value for $\langle\Delta\nu\rangle$ is the one that makes the $l = 0$ ridge vertical. Fig. 3 displays échelle diagrams for the two stars. To avoid ambiguity, the star with smaller $\langle\Delta\nu\rangle$ is named as KIC 7107778 A, and the larger one KIC 7107778 B. The best values are $\langle\Delta\nu\rangle_{\rm A} = 31.83 \pm 0.02$ μHz and $\langle\Delta\nu\rangle_{\rm B} = 34.55 \pm 0.01$ μHz.

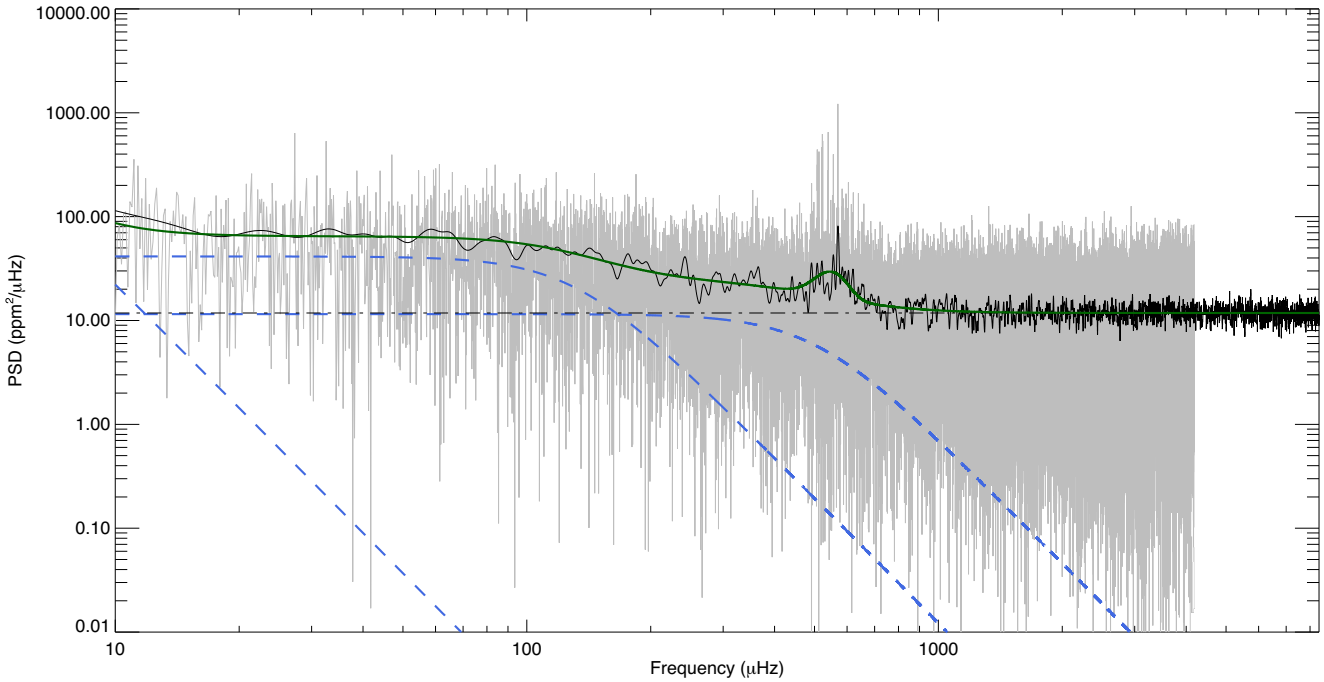

Figure 1. Power spectrum on a logarithmic scale. The solid grey line, the solid black line, the dashed blue lines, the dot–dashed-dashed black line, and the solid green line, outline the original power spectrum, the 6 μHz smoothed power spectrum, the Harvey profile components, the white noise component, and the total fitted power spectrum, respectively.

3 MODE PARAMETERS

To model the power spectrum, we used high-DImensional And multi-MOdal NesteD Sampling code (DIAMONDS; Corsaro & De Ridder 2014). The DIAMONDS code utilizes Bayes' theorem:

$$p(\theta \mid D, M) = \frac{\mathcal{L}(\theta \mid D, M)\pi(\theta \mid M)}{p(D \mid M)}, \tag{3}$$

where $\theta = (\theta_1, \theta_2, ..., \theta_k)$, $\mathcal{L}(\theta \mid D, M)$, $\pi(\theta|M)$, $p(\theta|D, M)$ are the parameter vector, likelihood function for a given model M and data set D, prior probability density function, and the posterior probability density function, respectively. DIAMONDS uses a sampling algorithm, Nested Sampling Monte Carlo, to tackle the high-dimensional problem.

We simultaneously fitted the two stars to separate their overlapping oscillations with the following steps. First, we modelled the power spectrum, $P(\nu)$, with

$$P(\nu) = W + R(\nu)\left\{\sum_{i=1}^{k}\frac{2\sqrt{2}}{\pi}\frac{a_i^2/b_i}{1+(\nu/b_i)^4} + H_0\exp\left[-\frac{(\nu-\nu_{\max})^2}{2\sigma^2}\right]\right\}, \tag{4}$$

similar to the background models presented in Kallinger et al. (2014) and Corsaro, De Ridder & García (2015). The right-hand side of the equation comprises a flat white noise W, a sum of Harvey power profiles (Harvey 1985) with parameters (a_i, b_i), and a Gaussian envelope with $(H_0, \nu_{\max}, \sigma)$. The Harvey profile models stellar background caused by granulation. In the case of KIC 7107778, the background was well fitted using three Harvey profiles, i.e. $k = 3$. The Gaussian envelope denotes the range of oscillation for two overlapping stars. All these components except the noise are modulated by the response function,

$$R(\nu) = \mathrm{sinc}^2\left(\frac{\pi\nu}{2\nu_{\mathrm{Nyq}}}\right), \tag{5}$$

where $\nu_{\mathrm{Nyq}} = 8496.36$ μHz denotes the Nyquist frequency. The total number of free variables is $1 + 2 \times 3 + 3 = 10$. The results are shown in Table 2. As argued by Kallinger et al. (2014), the granulation frequencies b_i should scale with $\nu_{\max}$. They provided empirical relations $b_2 = 0.317\,(\nu_{\max}/\mu\mathrm{Hz})^{0.970}$ μHz and $b_3 = 0.948\,(\nu_{\max}/\mu\mathrm{Hz})^{0.992}$ μHz, which result in $b_2 = 148.87$ μHz and $b_3 = 511.87$ μHz in our case. b_2 is similar to our fit but not b_3. This should be expected because the power spectrum is a superposition of the twins. b_1 should be treated carefully because the light curve was processed by a high-pass filter, which affected the low-frequency spectrum.

Then, each mode was fitted with a Lorentzian profile with three free parameters: frequency centroid ν_0, amplitude A, and linewidth Γ built on the background:

$$L(\nu) = R(\nu)\left[\frac{A^2/\pi\Gamma}{1+4\,(\nu-\nu_0)^2/\Gamma^2}\right]. \tag{6}$$

The power spectrum was fitted with a sum of 32 Lorentzian profiles. The total number of free variables is $3 \times 32 = 96$. It is possible that the star rotates and lifts degeneracy of m-degree of the modes (Gizon & Solanki 2003). Thus we performed a hypothesis test with Bayesian evidence denoted by $p(D|M)$ in equation (3). The Bayesian evidence balances the goodness of fit and the need to fit, as it can be written as a product of the maximum of the likelihood and an

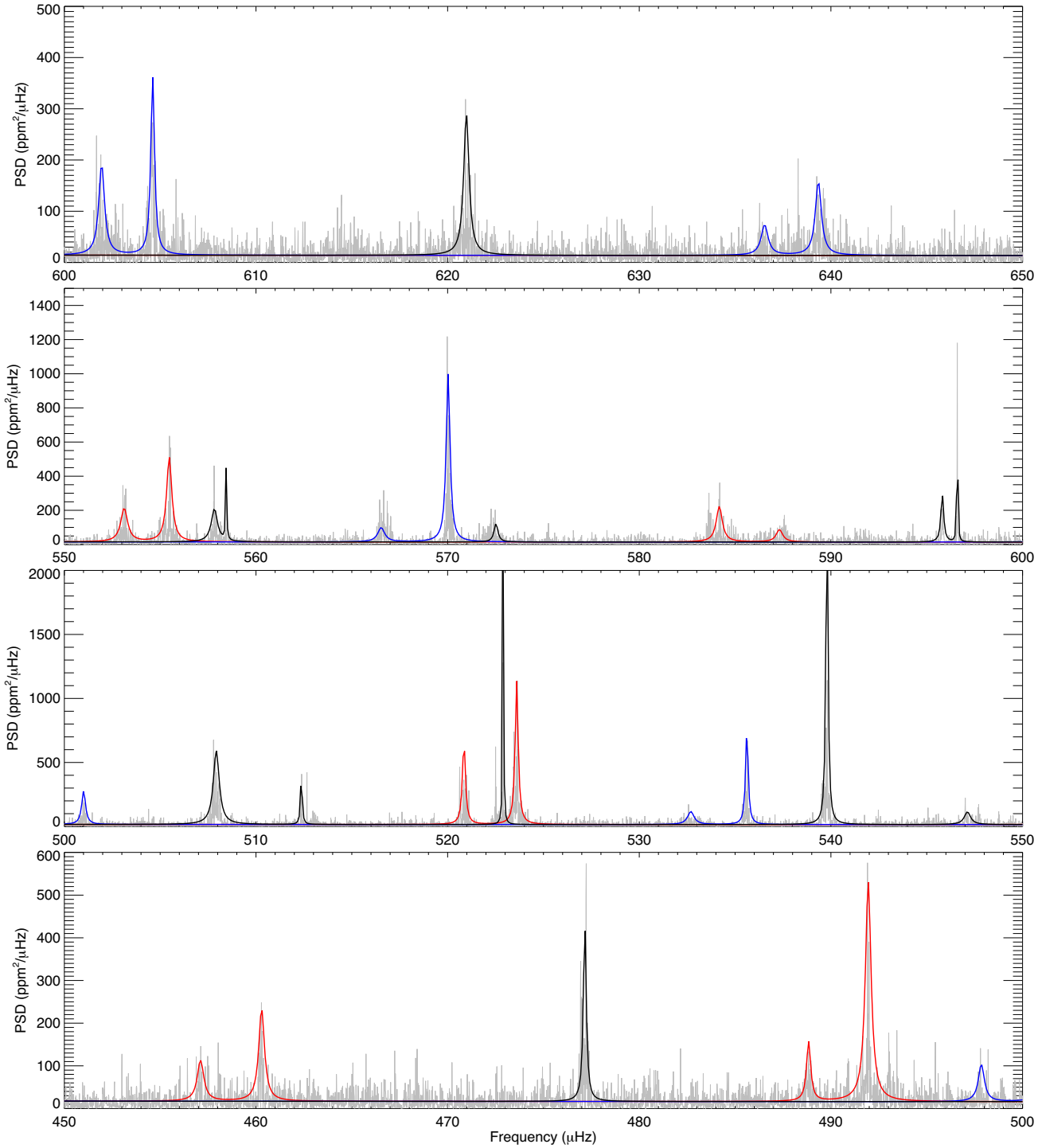

Figure 2. Power spectrum around the oscillation range on a linear scale. The grey line denotes the original power spectrum superimposed with fitted $l = 1$ modes in black, $l = 0$ and $l = 2$ modes of star A in red, and those of star B in blue.

Occam factor (Knuth et al. 2015). We adopted a splitting model of $l = 1$ modes

$$L(\nu) = R(\nu)\left[\sum_{m=-1}^{1} \frac{\xi_m A^2/\pi\Gamma}{1 + 4(\nu - \nu_0 - m\delta\nu_{\rm split})^2/\Gamma^2}\right], \quad (7)$$

where i is the inclination angle, $\xi_{-1} = \xi_1 = 0.5\sin^2 i$, $\xi_0 = \cos^2 i$, and $\delta\nu_{\rm split}$ measures the extent of splitting. We fitted the splitting model to four $l = 1$ modes (mode frequency 477, 507, 539, and 620 μHz) individually. The four modes were selected because they do not have another mode in 3 μHz frequency range. We defined detection probability as $p = p(D|M_{\rm B})/(p(D|M_{\rm A}) + p(D|M_{\rm B}))$ (Jeffreys

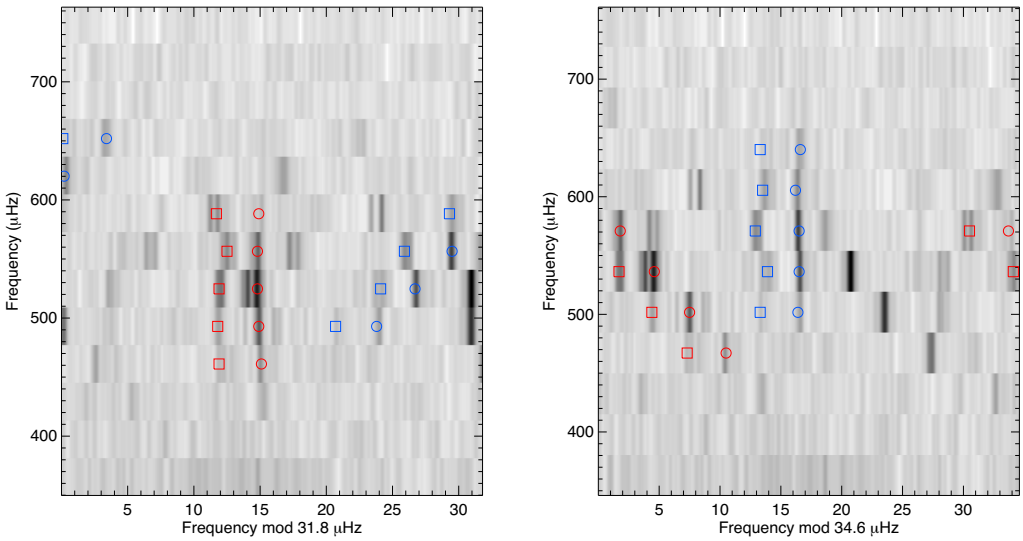

Figure 3. Échelle diagrams of star A (left) and star B (right). The circular and square open symbols represent identified $l = 0$ and $l = 2$ modes. Red and blue colours denote modes for star A and star B, respectively. The background grey-scale represents power density. Higher power density is shown darker. The unmarked peaks are $l = 1$ mixed modes.

Table 2. Granulation background parameters.

Parameter	Value	68.3 per cent credible
W (ppm^2 μHz^{-1})	11.927	0.100
a_1 (ppm)	58.874	8.314
b_1 (μHz)	5.203	1.460
a_2 (ppm)	67.167	8.705
b_2 (μHz)	149.144	32.207
a_3 (ppm)	76.134	7.947
b_3 (μHz)	400.646	64.318
H_0 (ppm^2 μHz^{-1})	17.977	2.852
$\nu_{\rm max}$ (μHz)	568.051	7.935
σ (μHz)	55.811	8.690

1961; Corsaro & De Ridder 2014), where subscripts A and B refer to the non-splitting model and the splitting model. The detection probabilities are small: 10^{-1}, 10^{-14}, 10^{-9}, and 10^{-2}, respectively. We also fitted the four modes with a common inclination and the detection probability is 10^{-50}. This indicates the non-splitting model gives a better depiction of the data. Hence, detecting the inclination angle i through rotation was not considered.

Notice that only $l = 0$ and $l = 2$ modes can be identified straightforwardly and allocated to one of the two stars, since they are regularly spaced. The $l = 1$ mixed modes are strongly bumped and no clear patterns could be followed, so we used stellar models to help the identification, as discussed in Section 4. We also measured the frequency of maximum power, $\nu_{\rm max}$, by fitting a Gaussian profile in power density to the $l = 0$ mode peaks. The results are $\nu_{\rm max,\,A} = 523 \pm 16$ μHz and $\nu_{\rm max,\,B} = 570 \pm 18$ μHz, where the uncertainties are half of $\langle\Delta\nu\rangle$.

Fig. 3 shows the échelle diagram of both stars. The circular and square open symbols represent identified $l = 0$ and $l = 2$ modes. Red and blue colours denote star A and star B, respectively. The mode parameters are shown in Tables 6 and 7. The $l = 1$ modes in the tables are further discussed in Section 4.3.

4 ASTEROSEISMIC ANALYSIS

As discussed in Section 2, KIC 7107778 has a long orbital period and no evidence of eclipses from which stellar fundamental parameters could be estimated. Therefore, estimating them through stellar models with asteroseismology is necessary.

4.1 Stellar models

We constructed stellar models using Modules for Experiments in Stellar Astrophysics (MESA; Paxton et al. 2011; Paxton et al. 2013; Paxton et al. 2015). Paxton et al. (2011) have discussed the input physics of MESA. Here we list them for completeness. The equation of state was delivered by OPAL EOS tables (Rogers & Nayfonov 2002), SVCH tables (Saumon, Chabrier & van Horn 1995) at low temperatures and densities, and HELM (Timmes & Swesty 2000) and PC (Potekhin & Chabrier 2010) tables under other circumstances. Opacities were taken from Iglesias & Rogers (1996) at high temperature and Ferguson et al. (2005) at low temperature. Nuclear reaction rates were based on NACRE (Angulo et al. 1999) and CF88 (Caughlan & Fowler 1988) when NACRE was unavailable. The convection was implemented with mixing length theory (MLT) illustrated in Cox & Giuli (1968). The mixing length parameter $\alpha_{\rm MLT} = 1.917$ was employed according to the MESA standard solar model (Paxton et al. 2011). Overshoot mixing was set according to Herwig (2000), with overshooting parameter $f_{\rm ov} = 0.016$. The initial helium abundance was estimated through

$$Y_{\rm ini} = Y_0 + \frac{\Delta Y}{\Delta Z} \cdot Z_{\rm ini}, \tag{8}$$

where $Y_0 = 0.249$ (Planck Collaboration XIII 2016) and $\Delta Y/\Delta Z = 1.33$, calculated using the initial abundances of helium and heavy elements of the calibrated solar model (Paxton et al. 2011). The relation of metallicity and element abundance ratio we adopted here was

$$[{\rm Fe/H}] = \log(Z/X) - \log(Z/X)_{\odot}, \tag{9}$$

Table 3. Input parameters of grid modelling.

	Value	Step size
M ($M_\odot$)	1.34–1.60	0.1
[Fe/H] (dex)	0.01–0.21	0.1
α_{MLT}	1.917	Fixed
f_{ov}	0.016	Fixed

where the solar value is $(Z/X)_\odot = 0.022\,93$ (Grevesse & Sauval 1998).

The varying input parameters for grid modelling are mass M and metallicity [Fe/H]. They were set as follows. First, the mass was set according to asteroseismic scaling relations. The mean large separation $\Delta\nu$ and frequency of maximum power ν_{max} are related to mean density ρ, surface gravity g, and effective temperature T_{eff}: $\Delta\nu \propto \sqrt{\rho}$, $\nu_{max} \propto g/\sqrt{T_{eff}}$ (Kjeldsen & Bedding 1995), i.e.

$$\frac{\Delta\nu}{\Delta\nu_\odot} \approx \left(\frac{M}{M_\odot}\right)^{1/2} \left(\frac{R}{R_\odot}\right)^{-3/2}, \tag{10}$$

$$\frac{\nu_{max}}{\nu_{max,\odot}} \approx \left(\frac{M}{M_\odot}\right) \left(\frac{R}{R_\odot}\right)^{-2} \left(\frac{T_{eff}}{T_{eff,\odot}}\right)^{-1/2}, \tag{11}$$

where $\Delta\nu_\odot = 135.1$ μHz, $\nu_{max,\odot} = 3050$ μHz (Chaplin & Miglio 2013) and $T_{eff} = 5777$ K. Thus, the mass prescription can be deduced from equations (10) and (11):

$$\frac{M}{M_\odot} \approx \left(\frac{\Delta\nu}{\Delta\nu_\odot}\right)^{-4} \left(\frac{\nu_{max}}{\nu_{max,\odot}}\right)^{3} \left(\frac{T_{eff}}{T_{eff,\odot}}\right)^{3/2}. \tag{12}$$

Considering the uncertainties, the mass range of the grid should at least cover 1.34–1.60 $M_\odot$. Secondly, we adopted metallicity [Fe/H] = 0.01, 0.11, and 0.21 according to spectral observations from LAMOST. Table 3 summarizes the input parameters of our grid modelling.

4.2 Modelling the $l = 0$ and $l = 2$ modes

We calculated oscillation frequencies for models that met the requirements of $\Delta\nu$ and ν_{max} with GYRE (Townsend & Teitler 2013), which solves the adiabatic pulsation equations with stellar structure data.

The calculated frequencies deviated from the observations due to the improper simulation of the stellar surface. Therefore, we followed the method described by Ball & Gizon (2014) to correct them. The correction formula we adopted here was

$$\delta\nu = (a_{-1}\nu^{-1} + a_3\nu^3)/I, \tag{13}$$

where a_{-1} and a_3 are coefficients determined through least-squares fit, and I is the mode inertia.

We used $\chi^2 = \Sigma(\nu_{obs} - \nu_{mod})^2/\sigma^2$ as the quality of the fit. Frequencies used in the χ^2 calculation were all $l = 0$ and $l = 2$ modes. The smaller the χ^2 of the model, the better the match. We took the best 10 per cent of the models, as measured by χ^2, for further considerations. The choice of this criterion was a trade-off. Small values could be biased by fluctuations in limited samples. The problem was tackled by sorting samples according to the values of χ^2, performing difference between two adjacent quantities. We found the trend around 10 per cent went smoothly, which ruled out the fluctuation effect. Including more models would make the selection less useful. This point was addressed by inspecting the value of χ^2 around the 10 per cent cut-off and assuring that it was not too large.

With the lowest 10 per cent χ^2 models, we calculated the mean value of the stellar parameters as the centroid. Table 4 lists them with standard deviations. Additionally, Figs 4 and 5 display histograms of each stellar parameter, which reflect the distribution in the lowest 10 per cent χ^2 models with [Fe/H] = 0.11. Red and blue indicate star A and star B, respectively.

Considering that [Fe/H] was estimated with uncertainties, we combined stellar parameters derived based on different [Fe/H] together, as the ultimate results. Here we list mass, radius, and age: $M_A = 1.42 \pm 0.06\ M_\odot$, $M_B = 1.39 \pm 0.03\ M_\odot$, $R_A = 2.93 \pm 0.05\ R_\odot$, $R_B = 2.76 \pm 0.04\ R_\odot$, $t_A = 3.32 \pm 0.54$ Gyr, and $t_B = 3.51 \pm 0.33$ Gyr.

4.3 Modelling the $l = 1$ mixed modes

We next searched for the best models which could also fit the frequencies of $l = 1$ modes from both stars. KIC 7107778 contains two sub-giant stars. Tiny changes to the mass of the models influence oscillations greatly. Only extremely fine grids produce satisfying results, which makes the task demanding. Since our purpose was to find a pair of stellar models for both stars that fit observations best, we used the bisection method to search.

The main idea of the bisection method is summarized as follows, similar to finding solutions for equation $f(x) = 0$. First, we started with two masses, M_1 and M_2, which lied on opposite sides of the best model. This choice was realized by visually inspecting oscillation frequencies on the échelle diagram. Secondly, we bisected this range, i.e. calculated frequencies of $M_3 = (M_1 + M_2)/2$. Thirdly, we evaluated the result of M_3 and determined M_3 and whichever of M_1 or M_2 yield the best model. Fourthly, we kept bisecting the mass range until the difference became sufficiently small.

Table 4. Fundamental properties of models from grid modelling.

Star	[Fe/H] (dex)	M ($M_\odot$)	Age (Gyr)	T_{eff} (K)	L ($L_\odot$)	R ($R_\odot$)	log g (dex)	$\Delta\nu$ (μHz)	ν_{max} (μHz)
A	0.01	1.41 ± 0.06	3.178 ± 0.440	5216 ± 258	5.813 ± 1.508	2.925 ± 0.047	3.654 ± 0.005	32.01 ± 0.18	534 ± 8
B	0.01	1.38 ± 0.03	3.289 ± 0.263	5233 ± 132	5.140 ± 0.692	2.754 ± 0.025	3.699 ± 0.003	34.77 ± 0.13	592 ± 5
A	0.11	1.43 ± 0.07	3.266 ± 0.583	5184 ± 290	5.787 ± 1.663	2.945 ± 0.055	3.656 ± 0.007	31.98 ± 0.17	539 ± 9
B	0.11	1.38 ± 0.03	3.606 ± 0.313	5092 ± 105	4.594 ± 0.549	2.751 ± 0.025	3.700 ± 0.004	34.81 ± 0.12	601 ± 4
A	0.21	1.41 ± 0.07	3.643 ± 0.551	5037 ± 199	5.032 ± 1.160	2.926 ± 0.054	3.655 ± 0.006	32.06 ± 0.15	546 ± 6
B	0.21	1.40 ± 0.04	3.657 ± 0.317	5045 ± 106	4.473 ± 0.535	2.765 ± 0.028	3.701 ± 0.003	34.78 ± 0.13	606 ± 4

Note. The models are selected with the lowest 10 per cent χ^2. Column 2 is the input parameter for grid modelling.

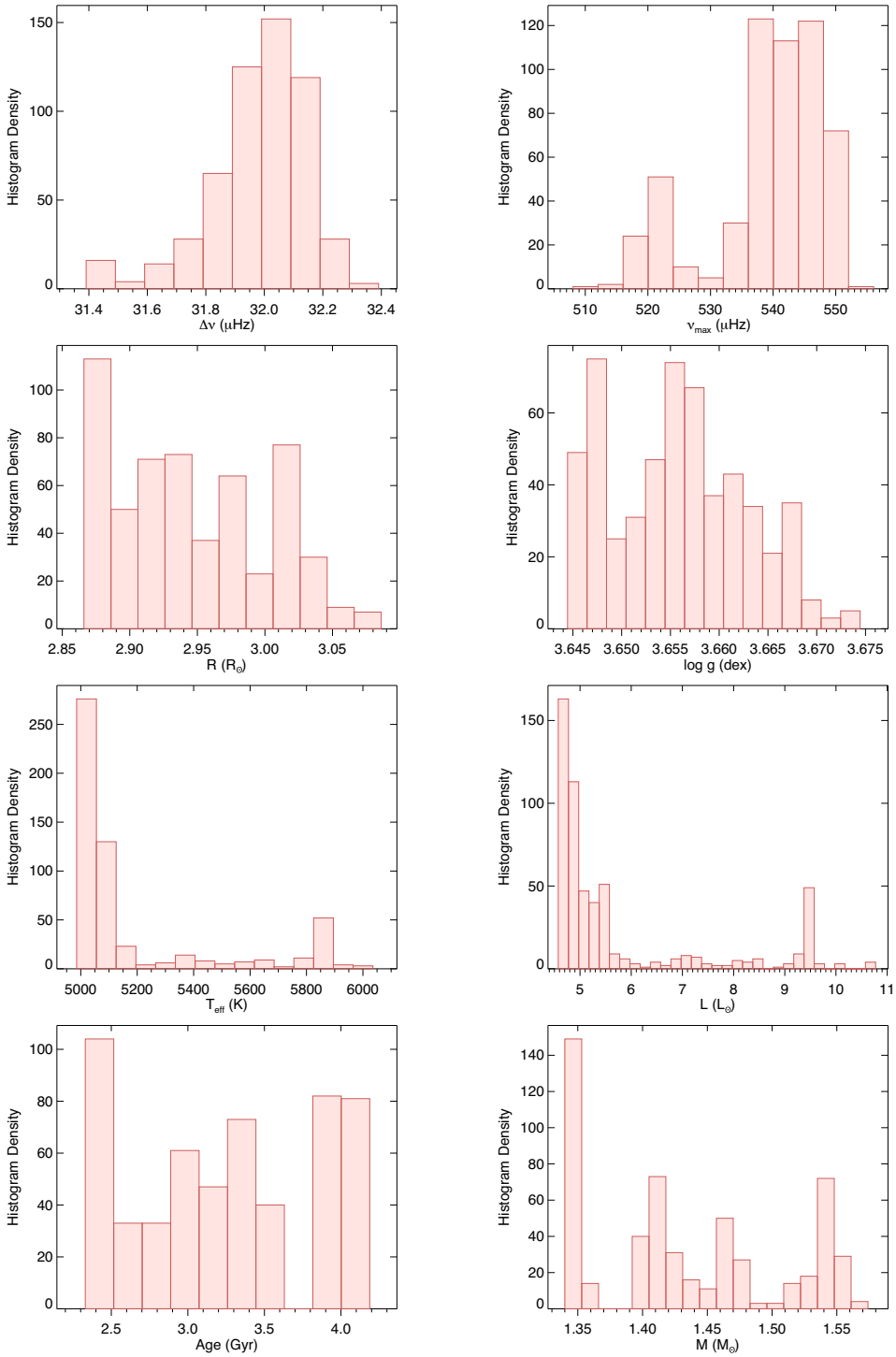

Figure 4. Parameter distributions for the lowest 10 per cent χ^2 of star A grid models with [Fe/H] = 0.11 dex.

We followed this search scheme under three different metallicities [Fe/H]: 0.01, 0.11, and 0.21. The maximum precision in calculation reaches 0.000 01 $M_\odot$. The results revealed three combinations of best-fitting models for the two stars. Although they do still deviate from observed peaks, they give a reasonable fit to most $l = 1$ modes. Most model masses reach to 0.001 $M_\odot$ precision. The reason of such small precision is that the mixed modes are very sensitive to the change of internal structure, and subgiants evolve very fast. Each combination has less than 0.2 Gyr difference in age, consistent with the idea that two components formed at the same time. Table 5 presents the fundamental parameters of the three model pairs, and Fig. 6 displays them on échelle diagrams. Open and filled symbols represent observational and theoretical frequencies. Red and blue indicate modes of star A and star B, respectively.

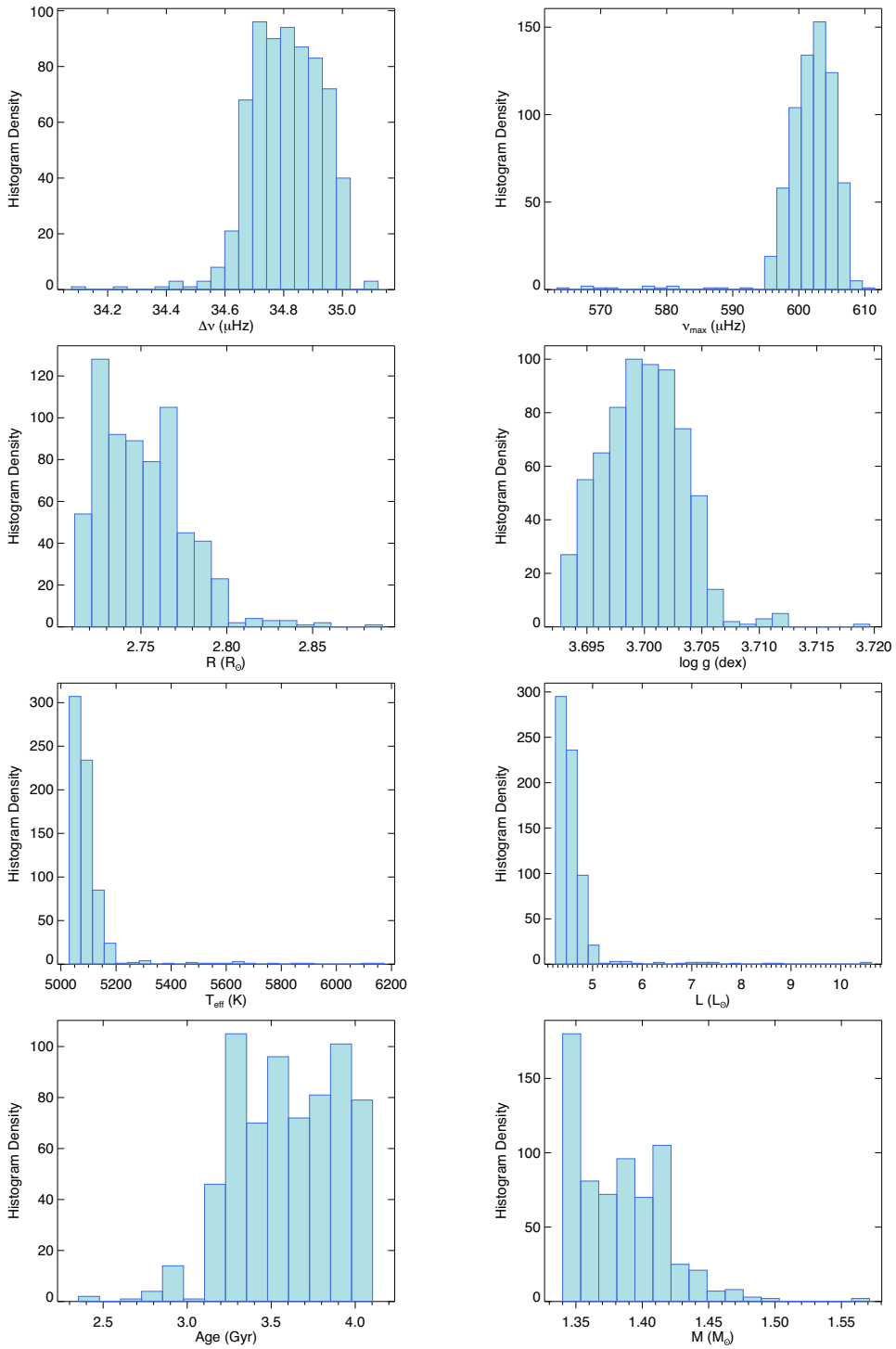

Figure 5. Parameter distributions for the lowest 10 per cent χ^2 of star B grid models with [Fe/H] = 0.11 dex.

Circles, squares, and triangles denote $l = 0$, $l = 1$, and $l = 2$ modes.

Based on theoretical models, we found that most observed peaks could be matched with $l = 1$ modes. Tables 6 and 7 display the mode parameters in each Lorentzian profile we fitted to each peak, with associated l degrees. Modes which share the same peak on the power spectrum are labelled with an asterisk mark. Some modes from the two stars stand too close and cause ambiguity; they are labelled with a question mark. Here we remind readers that this solution is not unique, considering that the models still differ from the observation. In Fig. 7, we show the mode linewidth as a function of the mode frequency. Mixed modes are expected to have smaller linewidths compared to radial modes because they have contributions from g modes trapped in the core, resulting a

Table 5. Fundamental properties of best models from bisection method.

No. #	Star	M ($M_\odot$)	[Fe/H] (dex)	Age (Gyr)	$T_{\rm eff}$ (K)	L ($L_\odot$)	R ($R_\odot$)	$\log g$ (dex)	$M_{\rm H,\,core}$ ($M_\odot$)	$\Delta\nu$ (μHz)	$\nu_{\rm max}$ (μHz)
1	A	1.41	0.01	3.063	5130	5.342	2.929	3.655	0.165	32.04	540
2	B	1.39	0.01	3.229	5195	4.982	2.759	3.699	0.157	34.74	594
3	A	1.48	0.11	2.873	5120	5.464	2.975	3.661	0.170	32.00	548
4	B	1.47	0.11	2.929	5267	5.478	2.814	3.705	0.162	34.64	599
5	A	1.42	0.21	3.533	4987	4.763	2.927	3.656	0.165	32.10	549
6	B	1.41	0.21	3.548	5038	4.443	2.770	3.703	0.160	34.80	608

Note. Columns 3 and 4 are the input parameters for grid modelling.

Table 6. Mode parameters of KIC 7107778 A.

l	Frequency (μHz)	68.3 per cent credible (μHz)	Amplitude (ppm)	68.3 per cent credible (ppm)	Linewidth (μHz)	68.3 per cent credible (μHz)		
0	460.294	$-0.022/+0.021$	15.66	$-0.80/+1.19$	0.36	$-0.09/+0.10$		
0	491.947	$-0.013/+0.014$	24.17	$-1.29/+1.66$	0.36	$-0.10/+0.13$		
0	523.603	$-0.012/+0.018$	25.84	$-1.85/+1.35$	0.19	$-0.07/+0.06$		
0	555.473	$-0.133/+0.090$	22.65	$-5.44/+2.56$	0.33	$-0.16/+0.18$		
0	587.314	$-0.420/+1.462$	9.65	$-2.24/+3.40$	0.41	$-0.17/+0.18$		
1	477.158	$-0.031/+0.042$	15.47	$-0.18/+0.25$	0.18	$-0.02/+0.02$		
1	488.837	$-0.022/+0.019$	10.70	$-0.48/+0.64$	0.26	$-0.09/+0.07$	*	
1	507.928	$-0.014/+0.013$	25.92	$-0.83/+0.99$	0.37	$-0.06/+0.06$		
1	522.897	$-0.002/+0.002$	21.55	$-0.75/+1.00$	0.04	$-0.01/+0.01$		
1	539.794	$-0.011/+0.008$	32.01	$-1.36/+2.02$	0.13	$-0.04/+0.05$		
1	558.446	$-0.172/+0.072$	9.08	$-3.06/+3.49$	0.06	$-0.02/+0.04$		?
1	572.522	$-0.827/+0.844$	9.03	$-2.80/+4.84$	0.24	$-0.13/+0.09$		?
1	595.812	$-0.040/+0.042$	12.35	$-1.44/+2.36$	0.17	$-0.11/+0.08$		?
2	457.106	$-0.046/+0.041$	11.10	$-0.49/+0.40$	0.41	$-0.07/+0.07$		
2	488.837	$-0.022/+0.019$	10.70	$-0.48/+0.64$	0.26	$-0.09/+0.07$	*	
2	520.851	$-0.020/+0.024$	19.66	$-0.31/+0.64$	0.19	$-0.05/+0.04$	*	
2	553.122	$-0.321/+0.354$	16.27	$-2.43/+3.94$	0.43	$-0.16/+0.14$		
2	584.175	$-0.393/+0.370$	15.78	$-2.33/+2.80$	0.38	$-0.13/+0.14$	*	

Note. Modes which share the same peak on the power spectrum are labelled with '*' marks. Modes from two stars standing too close and causing ambiguity are denoted with '?' marks.

Table 7. Mode parameters of KIC 7107778 B.

l	Frequency (μHz)	68.3 per cent credible (μHz)	Amplitude (ppm)	68.3 per cent credible (ppm)	Linewidth (μHz)	68.3 per cent credible (μHz)		
0	501.006	$-0.019/+0.020$	14.08	$-0.55/+1.06$	0.24	$-0.07/+0.05$		
0	535.615	$-0.016/+0.017$	19.47	$-0.66/+0.94$	0.16	$-0.03/+0.04$		
0	570.025	$-0.146/+0.423$	27.22	$-6.39/+8.01$	0.24	$-0.11/+0.10$		
0	604.609	$-0.026/+0.022$	15.92	$-2.44/+1.51$	0.23	$-0.08/+0.11$		
0	639.344	$-0.076/+0.068$	13.11	$-0.74/+0.99$	0.38	$-0.11/+0.13$		
1	512.368	$-0.008/+0.012$	11.26	$-0.93/+1.19$	0.09	$-0.06/+0.04$		
1	520.851	$-0.020/+0.024$	19.66	$-0.31/+0.64$	0.19	$-0.05/+0.04$	*	
1	547.122	$-0.735/+2.480$	11.15	$-2.42/+4.08$	0.40	$-0.16/+0.17$		
1	557.829	$-0.177/+0.168$	15.37	$-5.30/+5.61$	0.39	$-0.19/+0.17$		?
1	584.175	$-0.393/+0.370$	15.78	$-2.33/+2.80$	0.38	$-0.13/+0.14$	*	
1	596.595	$-0.001/+0.001$	18.12	$-1.00/+1.37$	0.02	$-0.00/+0.01$		
1	620.979	$-0.049/+0.040$	16.97	$-1.01/+1.17$	0.33	$-0.07/+0.10$		
2	497.849	$-0.096/+0.091$	10.21	$-0.74/+0.89$	0.38	$-0.11/+0.12$		
2	532.691	$-0.342/+0.315$	11.42	$-1.28/+2.08$	0.41	$-0.14/+0.14$		
2	566.534	$-0.731/+0.830$	10.72	$-2.78/+7.32$	0.44	$-0.17/+0.30$		
2	601.946	$-0.106/+0.109$	14.16	$-0.93/+1.22$	0.36	$-0.10/+0.10$		
2	636.541	$-0.380/+0.493$	9.04	$-1.04/+1.20$	0.44	$-0.14/+0.13$		

Note. Modes which share the same peak on the power spectrum are labelled with '*' marks. Modes from two stars standing too close and causing ambiguity are denoted with '?' marks.

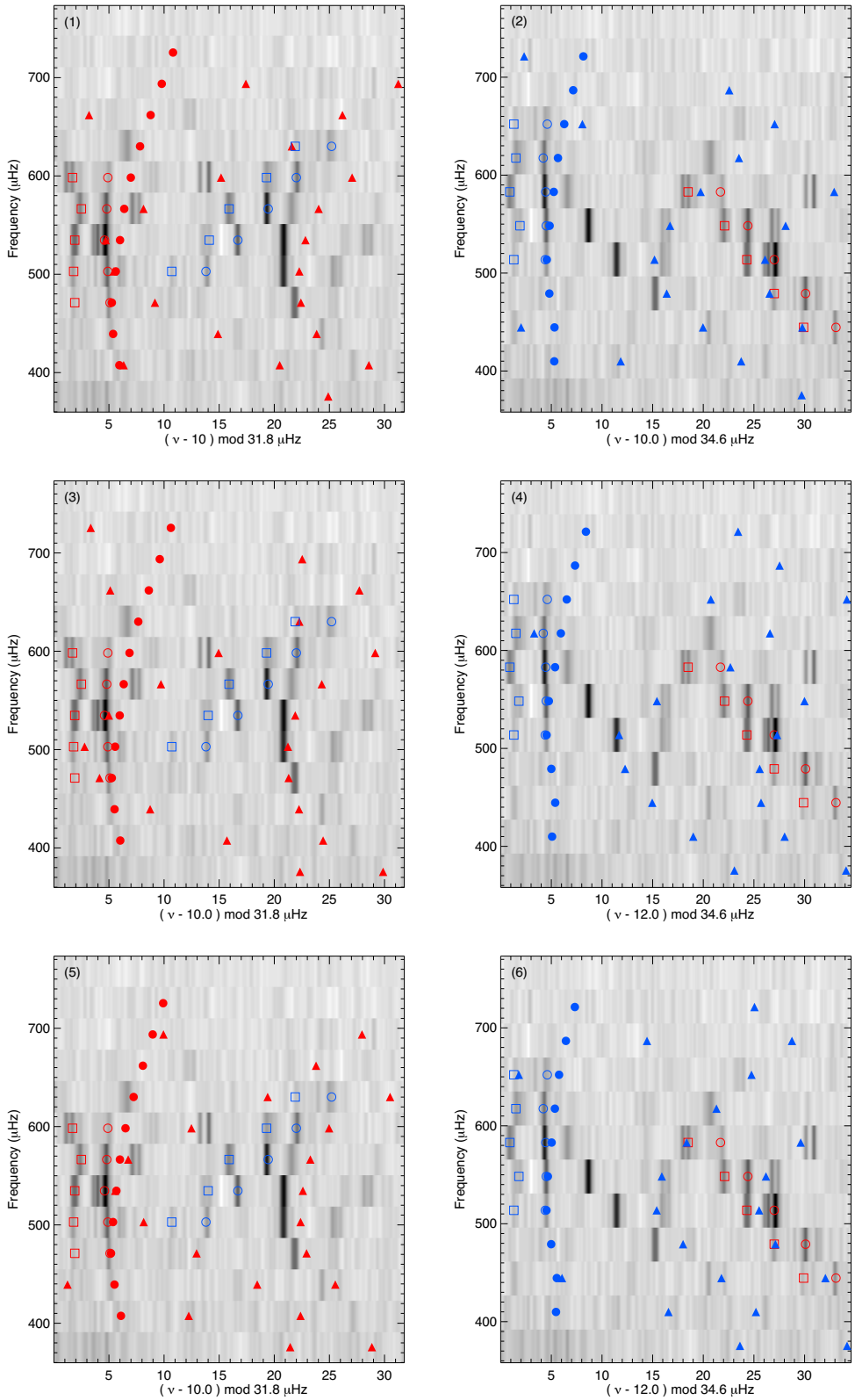

Figure 6. Échelle diagrams of KIC 7107778. Number series (1)–(6) on the upper left corner of each panel corresponds to the series of models in Table 5, whose oscillation frequencies are displayed in the corresponding échelle. These models are without surface corrections. Open and filled symbols represent observational frequencies and theoretical ones. Red and blue represent modes of star A and star B, respectively. Circles, triangles, and squares denote $l = 0$, $l = 1$, and $l = 2$ modes.

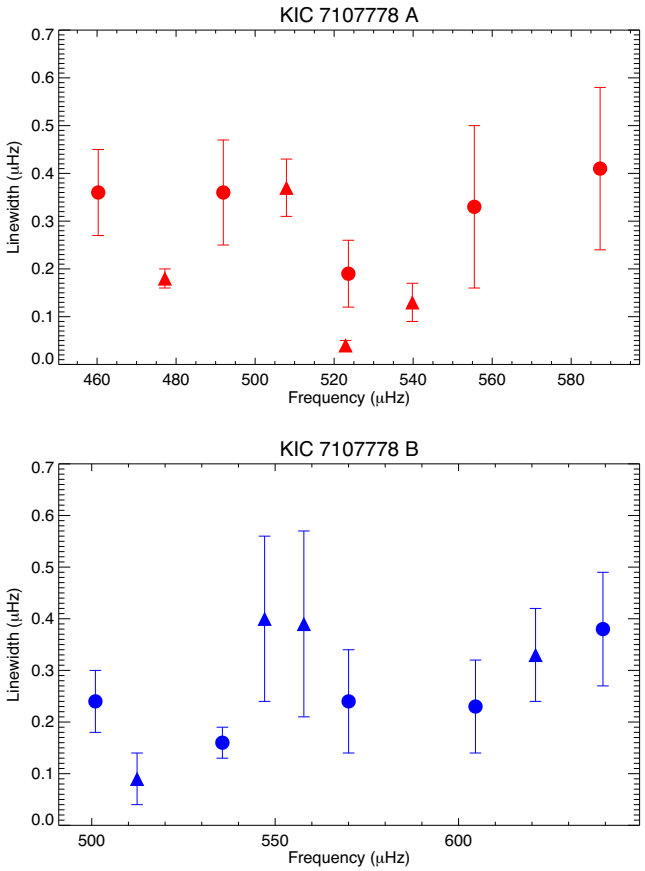

Figure 7. Mode linewidth as a function of mode frequency. The circles and triangles represent the $l = 0$ and $l = 1$ modes respectively. The $l = 1$ modes shown here are only those which have relative certain identity (not associated with '?' or '*' in Tables 6 and 7). The $l = 2$ modes are instead not presented because each $l = 2$ mode region is fitted with a Lorentzian profile, the linewidth of which is not necessarily representing the real mode lifetime.

longer lifetime (Dupret et al. 2009; Benomar et al. 2013). This is strongest for the mode at 522.897 μHz. For other $l = 1$ modes, the linewidths are similar to $l = 0$ modes because they are less bumped and more p-like.

Fig. 8 is the Hertzsprung–Russel diagram where grid and additional models are displayed with dotted black lines. Specifically, the dashed lines indicate the best model tracks from the bisecting method with star A in red and star B in blue, respectively. The star symbols denote the best models. The boxes consisting of solid lines indicate the standard deviation of effective temperature $T_{\rm eff}$ and luminosity L, shown in Table 4. The left-hand, middle, and right-hand panels represent models for metallicity [Fe/H] 0.01, 0.11, and 0.21.

5 CONCLUSION

We applied asteroseismology to a binary target KIC 7107778, and confirmed that the two stars are in the sub-giant phase. We successfully identified their $l = 0$ and $l = 2$ oscillation modes and distinguished $l = 1$ modes to the greatest extent. We derived stellar fundamental parameters for the two stars: $M_{\rm A} = 1.43^{+0.08}_{-0.08}$ $M_\odot$, $M_{\rm B} = 1.40^{+0.05}_{-0.06}$ $M_\odot$, $R_{\rm A} = 2.94^{+0.06}_{-0.06}$ $R_\odot$, $R_{\rm B} = 2.77^{+0.04}_{-0.04}$ $R_\odot$, $t_{\rm A} = 3.19^{+0.60}_{-0.64}$ Gyr, and $t_{\rm B} = 3.26^{+0.40}_{-0.40}$ Gyr. All the evidence suggests that they formed at the same time and possess nearly equal masses.

The results yield the similarity of masses for two stars, and the best models, derived through bisection modelling, determined the mass difference as 1.42 per cent, 0.68 per cent, and 0.70 per cent, from which we conclude it is ∼1 per cent. The H–R diagram verifies this, with extremely close tracks.

Table 4 indicates the sensitivity of metallicity to age, and the two stars' ages are equal within the error. We could conclude that they formed at the same time, as is expected by binary formation that they originate from the same protostellar cloud.

The KIC 7107778 system contains two extremely similar components, with fully overlapping power spectra. This is one of the few identical twin systems to be found, proving the full potential of asteroseismology.

ACKNOWLEDGEMENTS

We acknowledge the data from the *Kepler* Discovery mission, whose funding is provided by NASA's Science Mission Directorate. This work has also made use of data from the European Space Agency

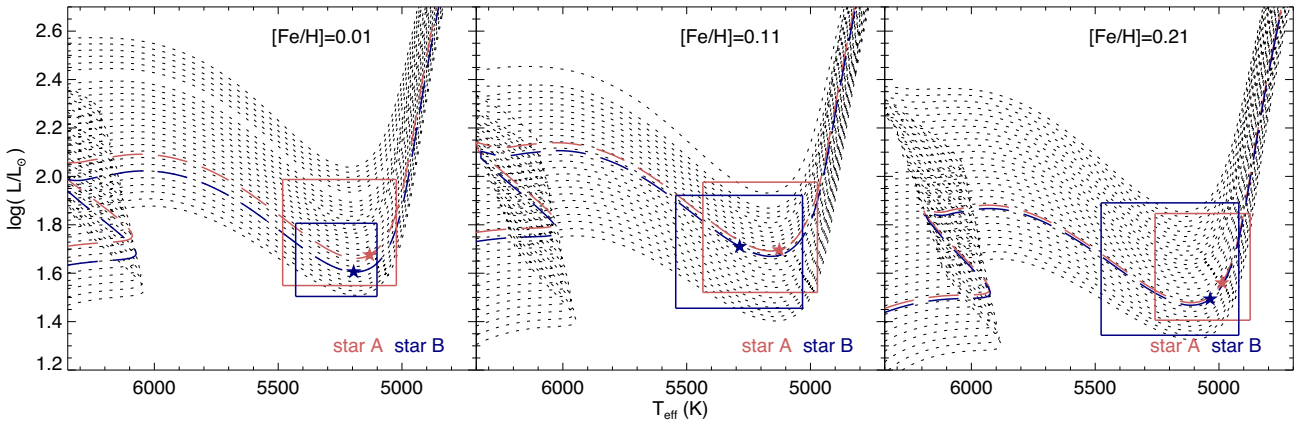

Figure 8. Hertzsprung–Russell diagram. Grid model tracks are displayed as black dotted lines. The best models, derived through bisection, are drawn with star symbols located on evolutionary tracks (dashed lines) in red for star A and in blue for star B. The solid lines indicate the standard deviation of effective temperature $T_{\rm eff}$ and luminosity L, which are shown in Table 4. The left-hand, middle, and right-hand panel represent models for metallicity [Fe/H] 0.01, 0.11, and 0.21, respectively.

(ESA) mission *Gaia*,[1] processed by the *Gaia* Data Processing and Analysis Consortium (DPAC[2]). Funding for the DPAC has been provided by national institutions, in particular the institutions participating in the *Gaia* Multilateral Agreement. S.B. and Y.L. acknowledges the Joint Research Fund in Astronomy (U1631236) under cooperative agreement between the National Natural Science Foundation of China (NSFC) and Chinese Academy of Sciences (CAS), NSFC 11273007 and 10933002, and the Fundamental Research Funds for the Central Universities. EC has received fundings from the European Union's Horizon 2020 research and innovation programme under the Marie Sklodowska-Curie grant agreement no. 664931.

REFERENCES

Aizenman M., Smeyers P., Weigert A., 1977, A&A, 58, 41
Andersen J., 1991, A&AR, 3, 91
Angulo C. et al., 1999, Nucl. Phys. A, 656, 3
Appourchaux T. et al., 2012, A&A, 543, A54
Appourchaux T. et al., 2014, A&A, 566, A20
Appourchaux T. et al., 2015, A&A, 582, A25
Ball W. H., Gizon L., 2014, A&A, 568, A123
Bate M. R., 2009, MNRAS, 392, 590
Bedding T. R., Kjeldsen H., Frandsen S., dall T. H., 1998, in Deubner F.-L., Christensen-Dalsgaard J., Kurtz D., eds, Proc. IAU Symp. 185, New Eyes to See Inside the Sun and Stars. Astron. Soc. Pac., San Francisco, p. 285
Benomar O., Bedding T. R., Stello D., Deheuvels S., White T. R., Christensen-Dalsgaard J., 2012, ApJ, 745, L33
Benomar O. et al., 2013, ApJ, 767, 158
Bouchy F., Carrier F., 2001, A&A, 374, L5
Buchhave L. A., Latham D. W., 2015, ApJ, 808, 187
Carrier F., Bourban G., 2003, A&A, 406, L23
Casagrande L., Ramírez I., Meléndez J., Bessell M., Asplund M., 2010, A&A, 512, A54
Caughlan G. R., Fowler W. A., 1988, At. Data Nucl. Data Tables, 40, 283
Chaplin W. J., Miglio A., 2013, ARA&A, 51, 353
Chaplin W. J. et al., 2014, ApJS, 210, 1
Corsaro E., De Ridder J., 2014, A&A, 571, A71
Corsaro E., De Ridder J., García R. A., 2015, A&A, 579, A83
Cox J. P., Giuli R. T., 1968, Principles of Stellar Structure. Gordon and Breach, New York
Drimmel R., Cabrera-Lavers A., López-Corredoira M., 2003, A&A, 409, 205
Dupret M.-A. et al., 2009, A&A, 506, 57
Fabricius C. et al., 2016, A&A, 595, A3
Ferguson J. W., Alexander D. R., Allard F., Barman T., Bodnarik J. G., Hauschildt P. H., Heffner-Wong A., Tamanai A., 2005, ApJ, 623, 585
Gaia Collaboration, 2016, A&A, 595, A2
García R. A. et al., 2011, MNRAS, 414, L6
Gizon L., Solanki S. K., 2003, ApJ, 589, 1009
Grevesse N., Sauval A. J., 1998, Space Sci. Rev., 85, 161
Harvey J., 1985, in Rolfe E., Battrick B., eds, ESA Special Publication Vol. 235, Future Missions in Solar, Heliospheric & Space Plasma Physics. ESA, Paris
Herwig F., 2000, A&A, 360, 952
Horch E. P., Howell S. B., Everett M. E., Ciardi D. R., 2012, AJ, 144, 165
Huber D., 2015, in Ake T. B., Griffin E., eds, Astrophysics and Space Science Library, Vol. 408, Giants of Eclipse: The Zeta Aurigae Stars and Other Binary Systems. Springer-Verlag, Berlin, p. 169
Iglesias C. A., Rogers F. J., 1996, ApJ, 464, 943
Jeffreys H., 1961, Theory of Probability. International Series of Monographs on Physics. Oxford Univ. Press, Oxford
Kallinger T. et al., 2010, A&A, 522, A1
Kallinger T. et al., 2014, A&A, 570, A41
Keen M. A., Bedding T. R., Murphy S. J., Schmid V. S., Aerts C., Tkachenko A., Ouazzani R.-M., Kurtz D. W., 2015, MNRAS, 454, 1792
Kjeldsen H., Bedding T. R., 1995, A&A, 293
Kjeldsen H., Bedding T. R., Frandsen S., dall T. H., 1999, MNRAS, 303, 579
Knuth K. H., Habeck M., Malakar N. K., Mubeen A. M., Placek B., 2015, Digit. Signal Process., 47, 50
Lomb N. R., 1976, Ap&SS, 39, 447
Lucy L. B., 2006, A&A, 457, 629
Lucy L. B., Ricco E., 1979, AJ, 84, 401
Metcalfe T. S. et al., 2010, ApJ, 723, 1583
Metcalfe T. S. et al., 2012, ApJ, 748, L10
Metcalfe T. S., Creevey O. L., Davies G. R., 2015, ApJ, 811, L37
Miglio A., Chaplin W. J., Farmer R., Kolb U., Girardi L., Elsworth Y., Appourchaux T., Handberg R., 2014, ApJ, 784, L3
Murphy S. J., Shibahashi H., 2015, MNRAS, 450, 4475
Murphy S. J., Bedding T. R., Shibahashi H., Kurtz D. W., Kjeldsen H., 2014, MNRAS, 441, 2515
Paxton B., Bildsten L., Dotter A., Herwig F., Lesaffre P., Timmes F., 2011, ApJS, 192, 3
Paxton B. et al., 2013, ApJS, 208, 4
Paxton B. et al., 2015, ApJS, 220, 15
Planck Collaboration XIII, 2016, A&A, 594, A13
Potekhin A. Y., Chabrier G., 2010, Contrib. Plasma Phys., 50, 82
Rogers F. J., Nayfonov A., 2002, ApJ, 576, 1064
Saumon D., Chabrier G., van Horn H. M., 1995, ApJS, 99, 713
Scargle J. D., 1982, ApJ, 263, 835
Schmid V. S. et al., 2015, A&A, 584, A35
Shibahashi H., Kurtz D. W., 2012, MNRAS, 422, 738
Simon M., Obbie R. C., 2009, AJ, 137, 3442
Tassoul M., 1980, ApJS, 43, 469
Timmes F. X., Swesty F. D., 2000, ApJS, 126, 501
Tokovinin A. A., 2000, A&A, 360, 997
Townsend R. H. D., Teitler S. A., 2013, MNRAS, 435, 3406
White T. R. et al., 2017, A&A, 601, A82
Xiang M. S. et al., 2015, MNRAS, 448, 822

[1] http://www.cosmos.esa.int/gaia
[2] http://www.cosmos.esa.int/web/gaia/dpac/consortium

This paper has been typeset from a TEX/LATEX file prepared by the author.